

## Gallium K-edge x-ray absorption study on Mg-doped GaN

Y. C. Pan, S. F. Wang, W. H. Lee, M. C. Lee, W. K. Chen, W. H. Chen, L. Y. Jang, J. F. Lee, C. I. Chiang, H. Chang, K. T. Wu, and D. S. Lin

Citation: [Applied Physics Letters](#) **78**, 31 (2001); doi: 10.1063/1.1337636

View online: <http://dx.doi.org/10.1063/1.1337636>

View Table of Contents: <http://scitation.aip.org/content/aip/journal/apl/78/1?ver=pdfcov>

Published by the [AIP Publishing](#)

---

### Articles you may be interested in

[Core-level photoemission and near-edge x-ray absorption fine-structure studies of GaN surface under low-energy ion bombardment](#)

*J. Appl. Phys.* **95**, 5487 (2004); 10.1063/1.1707232

[Excimer-laser-induced activation of Mg-doped GaN layers](#)

*Appl. Phys. Lett.* **84**, 2515 (2004); 10.1063/1.1695436

[Identification of implantation-induced defects in GaN: A near-edge x-ray absorption fine structure study](#)

*Appl. Phys. Lett.* **82**, 1556 (2003); 10.1063/1.1559650

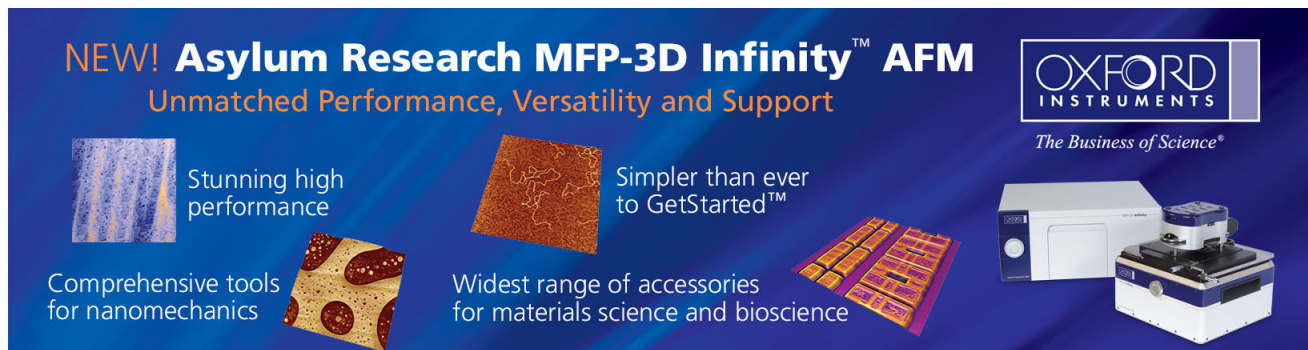
[Fluorescence x-ray absorption fine structure study on local structures around Fe atoms heavily doped in GaN by low-temperature molecular-beam epitaxy](#)

*Appl. Phys. Lett.* **78**, 2470 (2001); 10.1063/1.1368184

[Near edge x-ray absorption fine structure characterization of polycrystalline GaN grown by nitridation of GaAs \(001\)](#)

*J. Appl. Phys.* **86**, 209 (1999); 10.1063/1.370791

---

The advertisement features a dark blue background with white and orange text. At the top left, it says 'NEW! Asylum Research MFP-3D Infinity™ AFM' in large white letters, followed by 'Unmatched Performance, Versatility and Support' in orange. On the right is the Oxford Instruments logo with the tagline 'The Business of Science®'. Below the text are four images: a textured surface, a circular pattern, a grid of small squares, and the AFM instrument itself. Text descriptions are placed around these images: 'Stunning high performance' next to the textured surface, 'Simpler than ever to GetStarted™' next to the circular pattern, 'Comprehensive tools for nanomechanics' next to the grid, and 'Widest range of accessories for materials science and bioscience' next to the instrument.

## Gallium *K*-edge x-ray absorption study on Mg-doped GaN

Y. C. Pan, S. F. Wang, W. H. Lee, M. C. Lee, W. K. Chen, and W. H. Chen<sup>a)</sup>  
*Department of Electrophysics, National Chiao-Tung University, Hsin-Chu, Taiwan 300, Republic of China*

L. Y. Jang and J. F. Lee  
*Synchrotron Radiation Research Center, Hsin-chu, Taiwan 300, Republic of China*

C. I. Chiang and H. Chang  
*Chung-Shan Institute of Science and Technology, Tao-Yuan, Taiwan 325, Republic of China*

K. T. Wu  
*Department of Physics, Soochow University, Taipei, Taiwan 111, Republic of China*

D. S. Lin  
*Institute of Physics, National Chiao-Tung University, Hsin-Chu, Taiwan 300, Republic of China*

(Received 7 September 2000; accepted for publication 6 November 2000)

Ga *K*-edge x-ray absorption measurements were employed to investigate Mg-doping effects in GaN samples. Strong polarization-dependent x-ray absorption near-edge structures become less pronounced with increasing doping concentration, indicating the formation of a mixing-phase structure of cubic and hexagonal phases. Analysis of the extended x-ray absorption region of the spectra revealed doping-related defects such as vacancies, substitutions, and interstitial occupations. They were formed anisotropically in the crystal *c* axis direction and its perpendiculars. Disorderliness arising from phase mix and defects is believed to have lowered the Debye temperature of the doped GaN films and caused the destructive interference of the absorption fine-structure oscillation functions. These effects were taken into account for the observed large coordination number reductions in our samples. © 2001 American Institute of Physics.  
[DOI: 10.1063/1.1337636]

With wide direct-band-gap and high thermal stability, group-III nitride semiconductors are commonly used in short-wavelength light emitters and detectors as well as high-temperature and high-power electronic devices.<sup>1,2</sup> One of the major obstacles in *p*-type GaN growth is the limitation of carrier concentration ( $<10^{18} \text{ cm}^{-3}$ ), which makes the fabrication of GaN-based laser diodes very difficult.<sup>3</sup> Until now, Mg has been known to be one of the best *p*-type dopants for GaN. However, owing to its low activation efficiency ( $<10\%$ ), an optimal Mg incorporation concentration generally requires more than  $10^{20} \text{ cm}^{-3}$  to meet device-fabrication quality. In such a high doping concentration, the hexagonal lattice can be distorted by local stress and stacking faults.<sup>4</sup> Recently, cubic-phase GaN and other doping-related defects were also reported in high doping samples.<sup>5–7</sup> In this letter, we examined our samples with x-ray absorption fine-structure (XAFS) measurements. The analysis of the data did not result in a clear result until model simulations were made in examining the possible cases.

Undoped and Mg-doped GaN samples (thickness  $\sim 0.5\text{--}1 \mu\text{m}$ ) were grown on (0001) sapphire substrates at a temperature of  $1075^\circ\text{C}$  by an atmospheric-pressure horizontal metalorganic vapor-phase epitaxy (MOVPE) reactor. For undoped GaN growth, trimethylgallium (TMGa) and ammonia ( $\text{NH}_3$ ) were used as the Ga and N precursors with flow rates of  $10.4 \mu\text{mol}/\text{min}$  and  $0.7 \text{ slm}$ , respectively. For doped GaN growth, a flow of bis(cyclopentadienyl)magnesium ( $\text{Cp}_2\text{Mg}$ ) from  $0.02$  to  $0.79 \mu\text{mol}/\text{min}$  was introduced. The Mg solid concentrations of all samples were estimated to be

from  $\sim 10^{16}$  to  $\sim 10^{20} \text{ cm}^{-3}$  from secondary ion mass spectrometry data.<sup>8</sup>

Ga *K*-edge XAFS measurements were performed at the wiggler beamline BL17C in the Synchrotron Radiation Research Center (SRRC) of Taiwan. The photon energy for the XAFS covered the range between  $10\,200$  and  $11\,300 \text{ eV}$ . The intensity of the incidence x ray was monitored by a  $\text{N}_2$ -filled ionization chamber and the fluorescence emitted from the sample was measured by an argon-filled Stern–Heald–Lytle detector. A Si(111) double-crystal monochromator with a  $0.5 \text{ mm}$  entrance slit was used. A Zn filter was inserted between the sample and the detector window to reduce the noise from scattering and to improve the spectrum quality.

Figures 1(a) and 1(b) depict the Ga *K*-edge x-ray absorption near-edge structure (XANES) spectra for GaN samples in the grazing (electric-field vector  $E \perp c$  axis) and normal ( $E \parallel c$  axis) incidence angles, respectively. The four samples examined are undoped (*u*-), lightly Mg-doped ( $\text{Cp}_2\text{Mg} = 0.02 \mu\text{mol}/\text{min}$ ,  $[\text{Mg}] \approx 10^{16} \text{ cm}^{-3}$ ), heavily Mg-doped ( $\text{Cp}_2\text{Mg} = 0.79 \mu\text{mol}/\text{min}$ ,  $[\text{Mg}] \approx 2 \times 10^{20} \text{ cm}^{-3}$ ), and amorphous (*a*-) GaN. We shall call the  $[\text{Mg}] \approx 2 \times 10^{20} \text{ cm}^{-3}$  sample “the No. 633 sample.” The reference sample, *a*-GaN, results in both Figs. 1(a) and 1(b) show independent polarization effects due to their amorphous characteristic. In contrast, the other three samples exhibit strong polarization effects. Similar polarization variations on group-III *K*-edge XANES were also observed for AlN and InN.<sup>9</sup> This is attributed to the anisotropic distribution of the *p*-partial density of states (*p*-DOS) in the conduction band along the hexagonal *c* axis and its perpendiculars.<sup>9</sup> In Figs. 1(a) and 1(b), the XANES intensity interference oscillations are seen to attenuate

<sup>a)</sup>Electronic mail: whchen@cc.nctu.edu.tw

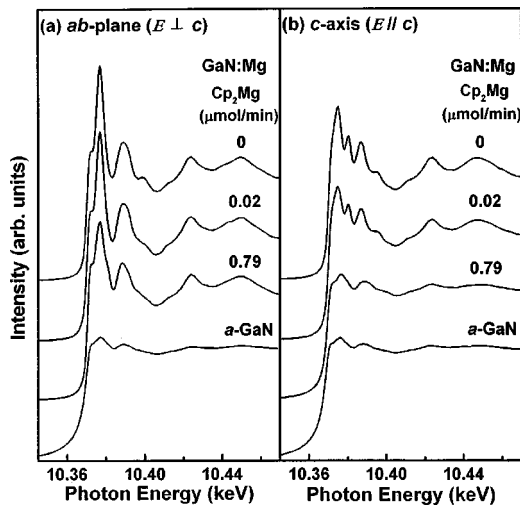


FIG. 1. Ga  $K$ -edge XANES spectra from undoped, lightly Mg-doped, heavily Mg-doped (No. 633), and amorphous GaN films in (a)  $ab$ -plane ( $E \perp c$ ) and (b)  $c$  axis ( $E \parallel c$ ) polarization modes.

ate with the increasing dopant concentration, suggesting that the electron density of the conduction band is decreased. This tendency is also consistent with PL results of an earlier report,<sup>10</sup> where the intensity of the near-band emission decreases as the Mg incorporation increases. We see the damping effect is more pronounced in the  $E \parallel c$  axis case than in the  $E \perp c$  axis case, revealing the influence of the Mg impurity on the  $p$ -DOS along the  $c$  axis direction is more significant than in the  $ab$  plane.

Extended XAFS (EXAFS) analyses of the samples were carried out using the FEFF7 program package<sup>11</sup> and the resulting Fourier transform (FT) magnitudes of  $k^2\chi(k)$  versus radial distance  $R$  for the cases of the  $E \perp c$  axis and  $E \parallel c$  axis are shown in Figs. 2(a) and 2(b), respectively. Again, the FT magnitude attenuation with the increasing Mg concentration is more pronounced in the  $E \parallel c$  axis than in the  $E \perp c$  axis. The first two shell distances,  $R_{\text{Ga-N}}$  and  $R_{\text{Ga-Ga}}$ , extracted from Figs. 2(a) and 2(b) using the FEFFIT fitting program for the two incident angles are shown in Figs. 3(a) and 3(b). The first-shell distance  $R_{\text{Ga-N}}$  slightly decreases as the Mg concentration increases in both polarization modes. Opposite to that, the second-shell distance  $R_{\text{Ga-Ga}}$  in Fig. 3(b) increases slightly. The shortening of  $R_{\text{Ga-N}}$  and the lengthening of  $R_{\text{Ga-Ga}}$  with the increasing dopant concentration can be understood qualitatively from the larger atomic radius of Mg than that of Ga.<sup>12</sup> In high concentration samples, more Mg atoms push N towards Ga, causing the reduction of  $R_{\text{Ga-N}}$ . The lengthening of  $R_{\text{Ga-Ga}}$ , however, would be caused by the bond-angle distortion in the normal GaN lattice.

Figures 3(c) and 3(d) show the first two shells' coordination numbers  $N_{\text{Ga-N}}$  and  $N_{\text{Ga-Ga}}$  in both polarization modes. They decline with the increasing Mg concentration, and the decline in the  $E \parallel c$  axis is more steep than in the  $E \perp c$  axis. One would first attribute this decline to the depletion of either nitrogen ( $V_{\text{N}}$ ) or gallium ( $V_{\text{Ga}}$ ) from their lattice sites during the Mg incorporation. These vacancy defects are energetically favored and easy to form.<sup>13</sup> Other than the declinations, we also noticed the coordination number reduction is rather anisotropic. In the first shell, the coordination numbers reduced from 2.0 to  $\sim 0.8$  and from 2.0 to  $\sim 1.4$  for the

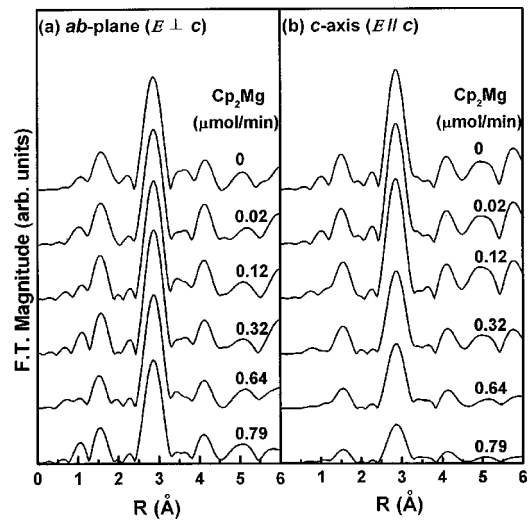


FIG. 2. Fourier transform (FT) magnitudes for Ga  $K$ -edge EXAFS from GaN films grown with various  $\text{Cp}_2\text{Mg}$  flow rates in (a)  $ab$ -plane ( $E \perp c$ ) and (b)  $c$  axis ( $E \parallel c$ ) polarization modes.

$E \parallel c$  axis and  $E \perp c$  axis, respectively, in the full concentration range. However, in the second shell, they reduced from 6.0 to  $\sim 2.1$  and from 6 to  $\sim 5.5$  for the two polarization modes, respectively. Based on our Raman results, the GaN crystalline structure is relatively well preserved.<sup>8</sup> Thus, we argue that these reductions must be due to reasons other than a simple great amount of vacancy defects.

To examine the possible causes for the observed coordination number reductions in the  $E \parallel c$  axis case, we took one step back to the comparison of  $k^2\chi(k)$  in the  $k$  space for the No. 633 data and the simulated curves of the models. In these  $k$ -power multiplied interference functions of  $\chi(k)$ , it is easier to see the envelope and frequency changes of the encompassed sinusoidal wave. We first compared our  $u$ -GaN  $k^2$ -multiplied data from AUTOBK and the  $k^2\chi(k)$  of the generated hexagonal GaN results in Fig. 4(a). AUTOBK is a back-

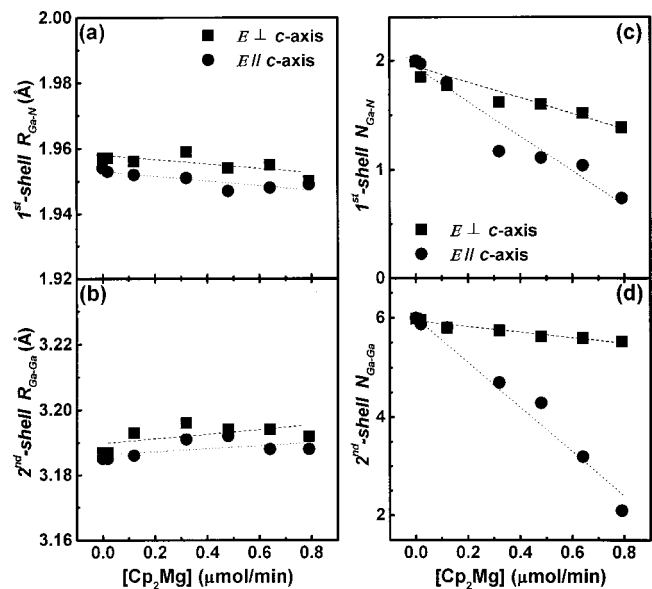


FIG. 3. (a) First-shell distances,  $R_{\text{Ga-N}}$ , (b) the second-shell distance,  $R_{\text{Ga-Ga}}$ , (c) the first coordination numbers,  $N_{\text{Ga-N}}$ , and (d) the second coordination numbers,  $N_{\text{Ga-Ga}}$ , as a function of dopant concentration in units of  $\text{Cp}_2\text{Mg}$  flow rate for the  $E \perp c$  axis (■) and the  $E \parallel c$  axis (●), respectively.

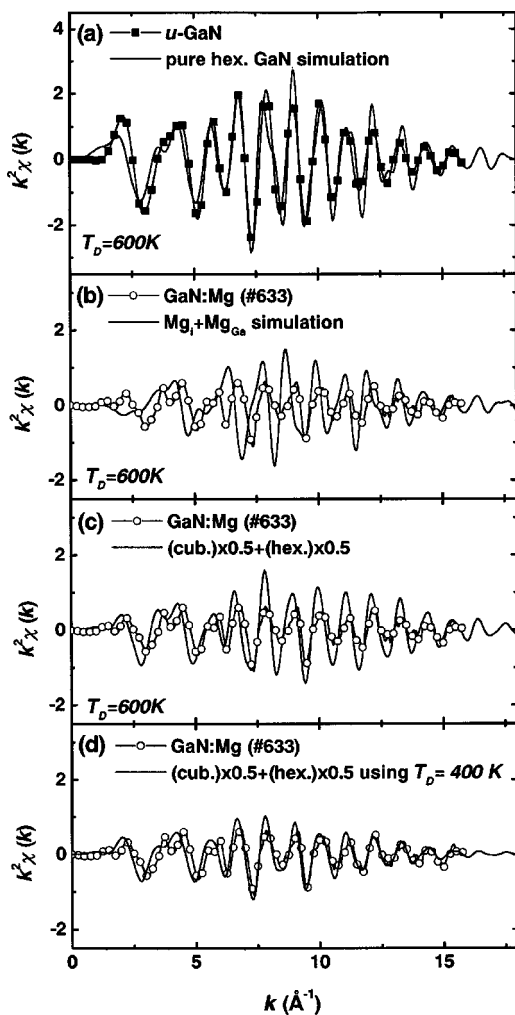


FIG. 4. Comparisons of  $k^2\chi(k)$  oscillations for the  $E\parallel c$  axis polarization of (a) our  $u$ -GaN and the FEFF7-generated undoped hexagonal GaN, (b) No. 633 GaN:Mg ( $[Mg]=2\times 10^{20}\text{cm}^{-3}$ ) and the simulated case of  $1Mg_i + 1Mg_{Ga}$ , (c) No. 633 and the simulation of mixed-phase  $1Mg_i + 1Mg_{Ga}$ , and (d) the case of (c) using reduced  $T_D=400\text{K}$ , showing the best fit of our data.

ground removal inclusion of FEFF7. The output file of ATOMS in FEFF7 provides a coordination list of atoms (relative to the absorber Ga atom at the origin) in a given crystal lattice. By alternating this coordination table, it is possible to simulate a number of cases such as vacancies ( $V_{Ga}$  and/or  $V_N$ ), substitutionals ( $Mg_{Ga}$ ), interstitial occupations ( $Mg_i$ ), as well as their combinations. In all these cases of  $1V_{Ga}$ ,  $1V_N$ ,  $1Mg_{Ga}$ ,  $1Mg_i$ ,  $2Mg_{Ga}$ , and  $2Mg_i$ , the amplitude drops for the  $k^2\chi(k)$  oscillations were found to be too small to match the observed No. 633 data, aside from frequency shifts for the interstitial cases. Because of the Mg concentration and the well-preserved crystalline form, impurity incorporation and vacancy defects larger than these cases would be impractical and were not attempted. However, the combination of one substitutional and one interstitial Mg ( $1Mg_{Ga} + 1Mg_i$ ) was able to provide comparable results in Fig. 4(b). The departure in frequencies of the two oscillations, however, was from the interstitial contribution. Additionally, from earlier reports,<sup>4,6</sup> we know that the cubic structure was induced by Mg incorporation to form mixed-phase GaN. Therefore, the  $1Mg_{Ga} + 1Mg_i$  cases for the hexagonal and the cubic GaN structures were generated separately and then superimposed

using the same weighting to simulate the mix-phase situation. A comparison of the resultant oscillation and the No. 633 data is given in Fig. 4(c). In this case, the phase shifting is seen to be reduced, but the theoretical oscillatory amplitude needs further suppression. To do this, one may consider the increasing disorderliness due to the presence of impurity-related defects and the formation of the mixed-phase structure in the film. This disorderliness in crystal lowered the lattice Debye temperature ( $T_D$ ) and decreased the Debye-Waller (DW) factor, resulting in reduction of the oscillatory amplitude. The simulation, including all these considerations, is shown in Fig. 4(d), where we have used  $T_D=400\text{K}$ , 50% weight for each phase, cubic  $Mg_i$  at (1.56, 1.56, and 1.56 Å) and hexagonal  $Mg_i$  at (0, 0, and 2.70 Å) with  $Mg_{Ga}$  for both crystals. After this, a better fitting was indeed obtained, except for a small phase difference at the low- $k$  region of the two oscillations.

In summary, the N  $K$ -edge XAFS measurements have revealed that Mg doping introduces substitutional and interstitial defects in GaN, and also results in the mixing of crystal phases. The disorderliness of the GaN film increases in proportion to the impurity content. As a consequence, the symmetry of the nitrogen electronic states in the conduction band becomes less defined, which results in structure blunting of the XANES spectra. The same reason causes the Debye temperature  $T_D$  to decrease, and thus brings down the  $k^2\chi(k)$  oscillatory amplitude, which is more pronounced in the  $E\parallel c$  axis case than in the  $E\perp c$  axis case. The optimal  $T_D$  to fit our No. 633 sample best is around 400 K, instead of the reported 600 K for  $u$ -GaN.<sup>14</sup> The destructive interference caused by substitutional and interstitial defects further reduces the amplitude. Decreases in FT magnitudes of the  $k^2\chi(k)$  functions in increasing Mg concentration then followed. Thus, the reduction in coordination numbers is not attributable to the vacancy defects on any significant scale.

The authors are grateful for the support by the National Science Council of the Republic of China under Contract Nos. NSC89-2112-M-009-012, NSC89-2112-M-009-013, and NSC89-2112-M-009-016.

- <sup>1</sup>S. Strite and H. Morkoç, J. Vac. Sci. Technol. B **10**, 1237 (1992).
- <sup>2</sup>H. Morkoç, S. Strite, G. B. Gao, M. E. Lin, B. Sverdlov, and M. Burns, J. Appl. Phys. **76**, 1363 (1994).
- <sup>3</sup>S. Nakamura, M. Senoh, S. Nagahama, N. Iwasa, T. Yamada, T. Matsushita, H. Kiyoku, Y. Sugimoto, T. Kozaki, H. Umemoto, M. Sano, and K. Chocho, Jpn. J. Appl. Phys., Part 2 **37**, L309 (1998).
- <sup>4</sup>S.-C. Y. Tsen, D. J. Smith, K. T. Tsen, W. Kim, and H. Morkoç, J. Appl. Phys. **82**, 6008 (1997).
- <sup>5</sup>M. Katsikini, T. D. Moustakas, and E. C. Paloura, J. Synchrotron Radiat. **6**, 555 (1999).
- <sup>6</sup>A. Cros, R. Dimitrov, H. Angerer, O. Ambacher, M. Stutzmann, S. Christiansen, M. Albrecht, and H. P. Strunk, J. Cryst. Growth **181**, 197 (1997).
- <sup>7</sup>D. H. Youn, M. Lachab, M. Hao, T. Sugahara, H. Takenaka, Y. Naoi, and S. Sakai, Jpn. J. Appl. Phys., Part 1 **38**, 631 (1999).
- <sup>8</sup>Unpublished data.
- <sup>9</sup>K. Lawniczka-Jablonska, T. Suski, Z. Liliental-Weber, E. M. Gullikson, J. H. Underwood, R. C. C. Perera, and T. J. Drummond, Appl. Phys. Lett. **70**, 2711 (1997).
- <sup>10</sup>B. Schineller, A. Guttzeit, P. H. Lim, M. Schwambera, K. Heime, O. Schön, and M. Heuken, J. Cryst. Growth **195**, 247 (1998).
- <sup>11</sup>J. Mustre de Leon, J. J. Rehr, S. I. Zabinsky, and R. C. Albers, Phys. Rev. B **44**, 4146 (1991).
- <sup>12</sup>S.-G. Lee and K. J. Chang, Semicond. Sci. Technol. **14**, 138 (1999).
- <sup>13</sup>J. Neugebauer and C. G. Van de Walle, Phys. Rev. B **50**, 8067 (1994).
- <sup>14</sup>G. A. Slack, J. Phys. Chem. Solids **34**, 321 (1973).